Time-Dependent Density-Functional Theory Investigation of the Fluorescence Behavior as a Function of Alkyl Chain Size for the 4-(*N*,*N*-Dimethylamino)benzonitrile-like Donor−Acceptor Systems 4-(*N*,*N*-Diethylamino)benzonitrile and 4-(*N*,*N*-Diisopropylamino)benzonitrile

Christine Jödicke Jamorski*,† and Mark E. Casida‡

Laboratorium für Physikalische Chemie, ETH Hoenggerberg, CH-8093 Zürich, Switzerland, and Laboratoire d'Études Dynamiques et Structurales de la Sélectivité (LÉDSS), Équipe de Chimie Théorique (LÉSS-ÉCT), Université Joseph Fourier (Grenoble I), 38041 Grenoble, France

Received: June 18, 2003; In Final Form: November 18, 2003

It has been observed experimentally that donor−acceptor systems of the same familly as 4-(*N*,*N*-dimethylamino)benzonitrile (4DMAB−CN) exhibit increased dual fluorescence activity as their alkyl chain length becomes longer. In the present study, the dual fluorescence activity of 4-(*N*,*N*-diethylamino)benzonitrile (4DEAB−CN) and 4-(*N*,*N*-diisopropylamino)benzonitrile (4DIAB−CN) molecules is investigated using time-dependent density-functional theory (TDDFT). Absorption and emission energies have been computed with the MPW1PW91 and the Becke three-parameter Lee−Yang−Parr (B3LYP) hybrid functionals in combination with the 6-311+G(2d,p) basis set. The ground-state geometry has been optimized at the B3LYP level with the 6-31G(d) basis set. The formation of the charge-transfer excited state has been examined from the point of view of the twisting intramolecular charge-transfer (TICT) and planar intramolecular charge-transfer (PICT) models previously proposed in the literature to explain the dual fluorescence behavior of this type of compound. Theoretical vertical excitation energies of 4DEAB−CN (4.45 eV and 4.56 with the B3LYP and MPW1PW91 functionals, respectively) compare well with the experimental value (4.35 eV) found in *n*-hexane. The abnormal L_a fluorescent band measured experimentally at 3.27 eV in *n*-hexane is well-produced by the MPW1PW91 vertical excitation energy (3.34 eV) computed for the twisted structure. For 4DIAB−CN, the MPW1PW91 absorption energy (4.21 eV) is in better agreement with that of the corresponding vapor phase (4.40 eV) than is the B3LYP result, as has already been observed for similar systems with pretwisted ground states (Jamorski, C.; Foresman, J. B.; Thilgen, C.; Lüthi, H.-P. *J. Chem. Phys.* **2002**, *116*, 8761). Emission from the twisted conformer is calculated at 3.40 eV (MPW1PW91) and 3.24 eV (B3LYP), both in good in agreement with the experimental gas-phase emission value (3.33 eV). No indication of a low-energy charge-transfer excited state is found when an investigation of potential energy surfaces is carried out within the geometrical constraints of the PICT model for the molecules studied here. It is found that, although TDDFT and DFT/MRCI methods yield results of comparable quality regarding absorption energies (DFT/MRCI results being better in the case of 4DIAB−CN), differences are observed when treating emission. Finally, the previous classification scheme previously established within the TICT model for this family of compounds (Joedicke Jamorski, C.; Lüthi, H.-P. *J. Chem. Phys.* **2003**, *119*, 12852) is also found to hold for the present systems, confirming the general validity of this scheme.

I. Introduction

The aim of this paper is to investigate the dual fluorescence experimentally observed for 4DEAB−CN and 4DIAB−CN molecules (see Figure 1) by exploring the potential energy surface of their ground and excited states along the twisting and wagging motion using time-dependent density-functional theory (TDDFT), which has demonstrated its capability in treating similar compounds,[1−6]

The dual fluorescence is a particular example of a more general process that involves the ability of systems to undergo a photoadiabatic reaction in the excited states (e.g., excited-state intramolecular proton transfer or double proton transfer). The first observation of the dual fluorescence phenomenon was reported forty years ago by Lippert et al.[7] in donor−acceptor systems such as 4-(*N*,*N*-dimethylamino)benzonitrile (4DMAB−CN); see Figure 2. Since then, this feature has been observed in a large variety of compounds such as nonsubstituted linear polyenes, as well as donor−acceptor systems, structurally similar to 4DMAB−CN. Furthermore, the nonlinear optical properties of these latter compounds has given rise to intensive research in the field of organic materials triggered by their possible application as electrooptical switches, chemical sensors, and

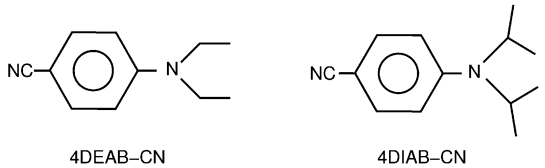

Figure 1. Molecules investigated in this study.

* Corresponding author. E-mail: christin@igc.phys.chem.ethz.ch.
† ETH Hoenggerberg.
‡ Université Joseph Fourier.

10.1021/jp0307699 CCC: $27.50
Published on Web 05/27/2004

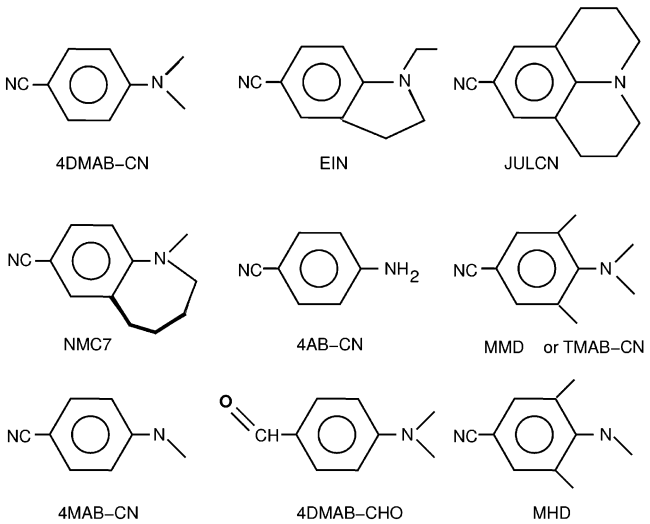

Figure 2. Molecules discussed in the text.

fluorescence probes.[8−10] Recently, the dual fluorescence property of donor−acceptor systems has been used in the fabrication of molecular switches.[11]

Experimentally, the fluorescence spectra consist of two bands. The normal band, L_b, shows a short axis polarization at the blue edge of the spectra, whereas a long axis polarization is observed for the rest of the spectra. The second band, L_a, also called abnormal emission in the literature, is red shifted and strongly solvent dependent compared to L_b. The presence and the behavior of this abnormal band have been explained by the existence of an intramolecular charge-transfer excited state with a large dipole moment. The L_b band is explained by an emission arising from the less polar locally excited (LE) state.

Since its first discovery, many scientists have been fascinated by this phenomenon and have tried to understand the mechanism of formation of the intramolecular charge-transfer excited state, as well as its final structure. Various mechanisms have been suggested, such as emission from two low-lying states and their inversion by interaction with the solvent proposed by Lippert et al.;[7] formation of an excimer;[12] proton transfer;[13] the rehybridization intramolecular charge-transfer model,[14−16] and complexation or formation of exciplexes with the solvent.[17,18] Today, mainly two models, the twisting and the planar intramolecular charge transfer are under debate. However, recent experimental and computational studies are predominantly in favor of the twisting model.

The first model proposed by Grabowski et al.,[19,20] commonly named TICT for twisting intramolecular charge transfer, supposes the existence of two conformers for the intramolecular charge-transfer excited state. After absorption, the promoted state starts in a nontwisted conformation. Then, in a radiationless process, it follows the hypersurface and transforms into a twisted structure, which is a local minimum on the potential energy surface along the rotation of the donor group with respect with the phenyl ring. Within this model, the final charge-transfer excited state presents a structure where the donor group is typically perpendicular to the phenyl ring, presenting thus a complete electronic decoupling. This model is based on the observation that only single fluorescence occurs for systems where the nitrogen of the donor group is prevented from rotating, such as in EIN and JULCN (see Figure 2).

A second model put forward by Zachariasse et al.,[21−26] under the acronym PICT for planar intramolecular charge transfer, has been proposed as an alternative. Originally, it was suggested to explain the presence of dual fluorescence in seven-membered ring systems,[21,25] like NMC7 (see Figure 2), in which the amino group cannot fully rotate, whereas single fluorescence is observed for five- and six-membered ring systems. This model supposes the existence of a solvent-induced vibronic coupling through the N-inversion mode of the amino group between the two initial singlet excited states, resulting in a more stable planar quinoidal structure for the charge-transfer excited state. In the PICT model, dual fluorescence should occur only for molecules that present a small energy gap between the two initial excited states to allow the vibronic coupling. Furthermore, only a small energy barrier to the rehybridization of the amino nitrogen from pyramidal to planar is allowed to permit the formation of the final planar ICT state.

No direct experimental proof for either model has been obtained up to now, indicating the need for detailed theoretical investigations to complement existant, and help to guide future, experimental work.

Recently, it has been possible to indirectly access the structure of the final charge-transfer excited state by measuring its infrared and Raman spectra. These techniques allow the measurement of the shift of specific vibrational frequencies associated with structural changes characterizing the final charge-transfer excited state. The time-resolved Raman spectra of the charge-transfer excited state of 4DMAB−CN has been reported by Kwok et al.,[27] who concludes in favor of the TICT model. Another study that combines CASSCF calculations and time-resolved vibrational spectroscopy[28] reaches the conclusion that no final statement between PICT or TICT can be made even though their results are in favor of the TICT model. The same conclusion is reached by the studies of Okamoto et al.[29−31] using picosecond infrared spectroscopy.

Theoretical chemists have tackled this problem using a myriad of methodologies that either include[28,32−42] or ignore[14−16,43−53] solvent effects. One of the precursory computational studies using a high level correlated method has been performed by Serrano et al.[45] They examined both models in detail for 4DMAB−CN and 4AB−CN (see Figure 2) using the complete active space with multiconfigurational second-order perturbation theory (CASPT2)[54,55] and inferred that only the twisting ICT model can explain the phenomenon. Several other investigations on the same compounds using various methods such as the similarity transform equation-of-motion coupled-cluster method with single and double excitations, STEOM-CCSD,[56,57] density-functional theory/single configuration interaction (DFT/SCI),[58] and DFT/multireference configuration of interaction (DFT/MRCI)[59] carried out by Parusel et al.[47−49] are also in favor of the twisting ICT mechanism. The same conclusion is drawn in the recent work of Sudholt et al.,[42] Mennuci et al.,[40] and Cammi et al.[41] on 4DMAB−CN, including solvent effects. Very recently, Furcher[60] optimized the geometry of the twisted charge-transfer excited state of 4DMAB−CN and successfully assigned the vibrational frequencies computed within the TDDFT method to the experimental spectra,[27,28] supporting therefore the twisting ICT hypothesis. The results of Parusel et al.,[53] who have computed the emission energies for the HF/CIS[61] and AM1/CISD optimized twisted intramolecular charge-transfer excited state using various methods (CASPT2, DFT/SCI, DFT/MRCI, and TDDFT) are in agreement with the experimental data, affirming the validity of the Twisting ICT Model.

Although 4DMAB−CN and 4AB−CN are the most investigated molecules from an experimental, as well as from a computational point of view, several other studies corroborating the twisting intramolecular charge transfer exist on systems such as phenylpyrole using the CASPT2 method[63] and N,N-

heterocyclic 4-aminobenzonitriles[50] and dicyano derivatives related to 4DMAB−CN,[52] both using the DFT/MRCI method. Zilberg and Haas[62] have recently performed a detailed investigations using the CASSCF and CIS methods of the optimized geometry of the excited states for several compounds and predict that the quinoid structure with a planar geometry corresponds to the PICT model, whereas the anti-quinoid structure with a perpendicular geometry conforms to the TICT model. Of particular interest to the present work is the recent investigation of Parusel et al.[51] on similar compounds (4DEAB−CN and 4DIAB−CN) using the DFT/MRCI method.

The present study is a new chapter of a series of papers in which we examine in detail the dual fluorescence for more than 21 molecules using the TDDFT method.[64−69] The assessment of the TDDFT method in computing vertical charge-transfer excited states for the family of donor−acceptor systems treated herein, is presented in ref 1. Both twisting and planar intramolecular charge-transfer models have been carefully explored for a set of dual and non dual fluorescent systems,[3] and our conclusion is in line with other theoretical investigations[45,47−49,53] reinforcing the twisting ICT model. The same general conclusion has been drawn after analyzing the effect of changing the donor and acceptor groups.[4,5] On the basis of the computed potential energy surfaces of the 21 examined donor−acceptor systems, we have proposed a classification in four groups based on three parameters (see Appendix for a summary). The fact that this classification reproduces the experimental fluorescence behavior is a strong indicaton for the validity of the TICT model.

It has been noticed that the ratio of quantum yields ϕ(CT)/ϕ(LE) increases with the length of the alkyl chain, and that compounds such as 4-(*N*,*N*-didecylamino)benzonitrile exhibit an intense dual fluorescence activity, even in nonpolar solvents, with a strong intensity observed for the L_a band; see ref 71. These observations have been interpretted differently by the TICT or PICT models. Within the TICT model, this increase in quantum yield has been attributed to an increase of the donor strength as the length of the alkyl chain becomes longer.[74] On the other hand, the PICT model attributes these observations to a smaller ΔE^{gap} between the first and second excited states, as well as to a larger pyramidalization angle of the nitrogen amino group as the alkyl chain length increases. These two arguments would favor the solvent−vibronic coupling, and therefore the existence of the charge-transfer state with a planar structure. The validity of the TICT model has been questionned[71] on the basis of the argument that rotation of the nitrogen amino should be more difficult for long alkyl chain compounds, which should therefore not exhibit a dual fluorescence activity, which is in disagreement with experiment. Recently, Zachariasse et al.[75] have observed that dual fluorescence occurs for 4DIAB−CN crystals and conclude that solvent is not necessarily important for the apperance of this phenomenon. This experiment opens new questions regarding the mechanism of formation of the ICT state in crystal structures, because the atoms are presumably fixed in place. Our calculations will be compared to gas-phase or liquid fluorescence measurements, only.

In this paper, we investigate, according to the planar and twisting intramolecular charge-transfer mechanism, the dual fluorescence activity experimentally observed in *n*-hexane for 4DEAB−CN[71] and in both vapor phase and *n*-hexane for 4DIAB−CN.[72,73] Our results will be reviewed within the TICT model, in terms of the previous proposed classification and the fluorescence behavior of the present molecules will be compared to other systems belonging to the same group. This perspective offers the possibility to assess the classification, and therefore to reinforce the validity of the TICT model, especially for the present compounds, which have a long alkyl chain, compared to the other already investigated systems.

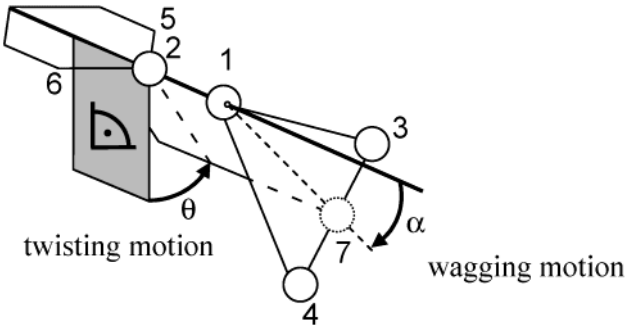

Figure 3. Schematic representation of the twisting and wagging motions investigated in this study. The ghost atom 7 is used in this figure to represent the "bissectrice" of the ∠314 angle.

II. Computational Details

All calculations have been performed using the GAUSSIAN 98 package.[76] 6-31G(d)[77] and 6-311+G(2d,p)[78,79] basis sets have been used in our calculations. These will be referred to later on, as Sm and Bg, respectively. Ground-state geometries have been optimized with the B3LYP[80] functional using the Sm basis set. Excitation energies were calculated at the B3LYP and MPW1PW91[81] levels in combination with the Bg basis set, using the TDDFT implementation in Gaussian.[82] Here, dipole moments for excited states were computed using the one-particle density matrix obtained by transforming the (X+Y) CI vectors into the atomic orbital basis (see Stratmann et al.[82] for the definition of X and Y).

In the text of this paper, the following general notation has been adopted: Opt-b1/Func-b2 where Opt stands for the functional used in the geometry optimization, Func for the functional used to calculate excited states, and b1, b2 specified the basis set in each case. This notation reduces to a shorter form when b1 = b2 or Opt = Func or Opt-b1 = Func-b2. For example, B3LYP−Sm/B3LYP−Bg will be written B3LYP−(Sm/Bg) and B3LYP−Sm/B3LYP−Sm will simply be written B3LYP−Sm. Also, the MPW1PW91-(Sm/Bg) notation has been written in the following abbreviated form MPW91-(Sm/Bg).

For all molecules, excitation energies are calculated low enough, compared to $-\epsilon_{HOMO}$, to be considered reliable.[83] Computed excitation energies are vertical excitation energies without zero-point energy correction.

The angles used in the text to define the geometry, as well as the investigated motion, are shown in Figure 3. The twisting motion of the TICT model is described by the variation of the angle θ from 0° to 180° with a step of 30° for molecules of this study. θ is defined by $(\theta_1 + \theta_2)/2$ where θ_1 represents the dihedral angle ∠4126 and θ_2 corresponds to ∠3125. For each fixed θ angle, a partial optimization of geometry of the donor group has been performed at the B3LYP−Sm level. The difference in excitation energies with or without partial optimization of geometry is on the order of 0.10 eV. In the literature, the term wagging angle has been used in various ways. In this paper, we describe the wagging motion used to modelize the PICT mechanism by the variation of the angle $\alpha' = \angle 712$, where $\overline{17}$ is defined to be the "bissectrice" of the angle ∠314, from its ground-state value. For the ease of comparison to our previous work and other papers, we alternatively utilize the dihedral angle, $\alpha = 180° - \angle 4123$, which we call the wagging angle. In most practical cases, α and α' only differ by a few

TABLE 1: Comparison between Experimental and TDDFT Absorption and Emission Energies (eV) Obtained with or without (Our Work) Optimization of Geometry of the Twisted Charge-Transfer Excited State of 4DMAB−CN[a]

	absorption						emission		
	1B ⇒ LE			1A ⇒ CT			TICT		
methods	ΔE	f	μ	ΔE	f	μ	ΔE	μ	ΔE^{1S} [b]
exp	4.25[c]			4.56[c]			3.2−3.3[d]		
TDDFT (Parusel)[e]	4.50	0.03		4.70	0.50		3.1		0.92[f]
TDDFT(our work with $\alpha = 0°$)[g]	4.35	0.03	11.81	4.60	0.53	14.63	3.09	20.16	0.67[h]
TDDFT (our work with $\alpha = 20°$)[i]	4.38	0.03	11.48	4.60	0.48	12.76	3.19[j]	20.15	0.77[k]

[a] See also refs 1, 3, and 4. Oscillator strength, f, and dipole moments, μ (D) are also reported. Our ground-state geometry has been optimized at the B3LYP−Sm level, and excitation energies have been computed using the B3LYP−Bg method. Our emission energies are calculated at the perpendicular ground-state geometry ($\theta = 90°$). [b] Energy difference between the charge-transfer excited state with a perpendicular structure and the first vertical excited state 1B. [c] Electron energy loss measurements.[43] [d] Measured in *n*-hexane.[71] In the gas phase, these values are expected to be higher (between 3.5 and 3.6 eV). [e] TDDFT calculations performed by Parusel et al.[53] using an optimized AM1/CISD ground-state geometry for the absorption energies and an optimized AM1/CISD excited state. Twisted geometry for the emission energies. [f] Energy difference between the optimized AM1/CISD excited TICT state and the vertical 1B excited state with an optimized AM1/CISD ground-state structure. [g] For the electronic ground state of 4DMAB-CN, the wagging angle is optimized at 0° using the Sm basis set with the B3LYP functional. [h] Energy stabilization of the TICT state ($\theta = 90°$) versus the 1B vertical excited state. [i] The wagging angle is fixed at 20°, the rest of the structure corresponding to the optimized ground-state geometry. [j] Emission energy calculated for a twisted and wagged ($\theta = 90°$, $\alpha = 20°$) structure; see ref 3 for more details. [k] Energy stabilization of the TICT state having a twisted and wagged ($\theta = 90°$, $\alpha = 20°$) structure versus the 1B vertical excited state with a ground-state structure being wagges by 20°.

degrees and α' can be found from α by simple geometrical considerations. In addition, we define the angle $\gamma = (\theta_1 - \theta_2)/2$, which is often given in the literature to describe the structure. In the text, the twisting and wagging angles referring to the value obtained for the optimized ground-state structure are symbolyzed by θ^0 and α^0, respectively.

This study is limited in the sense that it only corresponds to cuts of the PE hypersurface along the twisting and wagging angles and no full geometry optimization of the various excited states have been performed.[84−86] This approach, which uses the ground-state optimized geometry as a basis for the representation of the excited-state structure, has been successfully applied in many scientific publications.[45,57,49−51,53] It is possible to estimate its accuracy by comparing our results with the ones obtained by Parusel et al.,[53] who recently optimized the excited-state geometries using the AM1/CIS and HF/CIS methods for 4DMAB−CN. Table 1 compares our calculated absorption and emission energies computed for 4DMAB−CN with the ones of Parusel. The variation observed in absorption between these two approaches is due to different choices of basis sets and methods for optimizing the ground-state structure. Our emission energies, computed for two wagging angles ($\alpha = 0°$ and $\alpha = 20°$, experimentally $\alpha = 10.8°$ and $11.9°$ [87] in the solid and 15° in the gas phase[88,89]), are close to Parusel's results. Furthermore, our results correctly describe the gain in energy of the twisted charge-transfer excited state compared to the first vertical excited state. Therefore, we feel confident that the chosen approach provides a semiquantitative description of the emission energies, as well as of the form of the potential energy surface of the charge-transfer excited state.

This simple approach has shown its ability to predict the occurrence or absence of dual fluorescence activity for more than 21 molecules of the same family, in agreement with the experimental data. The reader is referred to refs 3 and 4 for more information about computational details.

III. Discussion

A. Structure and Molecular Orbitals. Table 2 gives the angle values of both optimized electronic ground-state structures obtained at the B3LYP level using the Sm basis set.

According to refs 51 and 90 the crystal structure of 4DEAB−CN is untwisted ($\theta = 0°$) and α' is given at 6°. On the basis of the analysis of the photoelectron spectra using first-order perturbation theory, Rettig et al.[90] have made an indirect measurement of the ground-state torsional angle, θ, for 4DEAB−CN in solution and predict a θ value of 21°. Our values for θ and α' are close to the ones found by Parusel et al.[51] ($\theta = 5.2°$ and $\alpha' = 0°$ using the same functional and the same quality basis set.

TABLE 2: Computed Angles θ, α', α, and γ (deg) for the B3LYP-Optimized Ground State of 4DEAB−CN and 4DIAB−CN Molecules Using the 6-31G(d) Basis Set

	4DEAB−CN			4DIAB−CN		
angles	our work	Parusel[a]	exp	our work	Parusel[a]	exp
θ	0.0	5.2	21;[b] 0[c]	38.0	32.2	9.45[d]
α'	3.22	0	6[c]	18.23	0.0	
α	3.88			19.33		
γ	0.0			10.16		14.9[d]

[a] Work done by Parusel; see ref 51. [b] The value of 21° for θ has been estimated in solution by Rettig et al.[90] [c] The crystal structure measurements; see ref 51 and ref 24 therein.[90] [d] Crystal structure measurements; see ref 72.

For 4DIAB−CN, Demeter et al.[72] obtained a slightly twisted crystal structure ($\theta = 9.45°$), whereas our calculations for the free molecule show a twisting angle of 38° close to the 32.2° obtained by Parusel. For this molecule, we compute $\alpha' = 18.23°$ in disagreement with Parusel's calculations ($\alpha' = 0°$). The value of 10.16° obtained for γ compares well to the experimental value of 14.9° measured by Demeter et al.

Molecular orbitals (MO) of the 4DEAB−CN molecule are displayed in Figure 4 at the equilibrium and perpendicular geometry. The 4DIAB−CN molecule MOs are qualitatively similar to those of 4DEAB−CN. The LUMO and LUMO+1 have a π^*_{acceptor} and a π^*_{phenyl} character, independent of the geometric conformation of the molecule. On the other hand, the HOMO shows a π_{donor} nature at the equilibrium ground-state geometry and a n_N character at the twisted conformer. The HOMO → LUMO electronic promotion is identified as the charge-transfer transition.

B. Absorption Spectra for 4DEAB−CN and 4DIAB−CN. Table 3 displays the experimental and calculated absorption and emission energies for 4DEAB−CN and 4DIAB−CN, as well as their corresponding computed dipole moments and oscillator strength.

For 4DEAB−CN, the B3LYP and MPW1PW91 computed dipole moments of the electronic ground state are in agreement

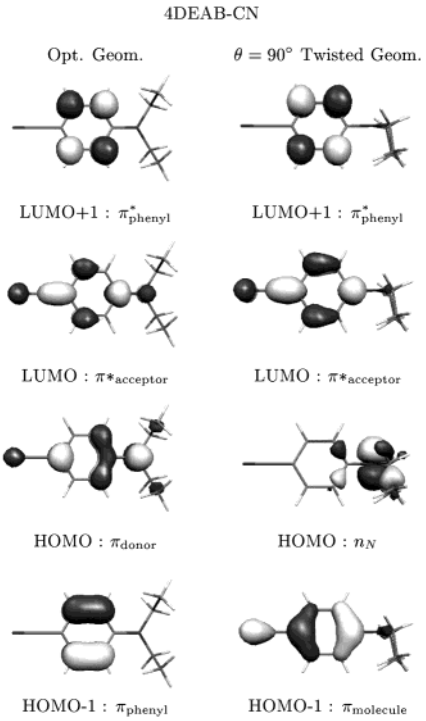

Figure 4. Molecular orbitals (MO) for the optimized ground-state structure and twisted conformers of 4DEAB−CN.

with the experimental one measured in dioxane.[70] The experimental spectrum of 4DEAB−CN has been recorded in *n*-hexane by Rettig,[91] who reports an absorption energy of 4.35 eV. The TDDFT computed absorption spectrum of 4DEAB−CN presents the same structure as the one of 4DMAB−CN, which serves as a model compound for this family of donor−acceptor systems. The first excited state, which has an oscillator strengh of 0.02, is associated with the $\pi_{donor} \rightarrow \pi^*_{phenyl}$ electronic promotion and is similar in nature to the 1B state observed in the absorption spectrum of 4DMAB−CN. The second excited state, which possesses a large oscillator strengh (0.47), corresponds to the charge-transfer excited state related to a $\pi_{donor} \rightarrow \pi^*_{acceptor}$ electronic transition and has a character comparable to the 2A excited state of 4DMAB−CN. Extending the alkyl chain size from 4DMAB−CN to 4DEAB−CN reduces the energy gap between the vertical first and second excited states from 0.25 to 0.14 eV, respectively, at the B3LYP level. Excitation energies computed with both B3LYP and MPW1PW91 functionals compare well to experimental measurements and to the DFT/MRCI values obtained by Parusel et al.[51] Adding a solvent energy shift of 0.2 eV to the *n*-hexane measurements (4.35 eV) leads to an estimated gas-phase value of 4.55 eV, which is in better agreement with the MPW1PW91 and DFT/MRCI (4.56 eV) computed excitation energy than with the B3LYP (4.45 eV) one.

In the case of 4DIAB−CN, the absorption spectra reported in *n*-hexane by Demeter et al.[72] and in vapor phase by Daum et al.[73] have been measured at 4.22 and 4.40 eV, respectively. Going from the dimethyl to the diisopropyl donor group yields a large stabilization of the charge-transfer excited state. The

TABLE 3: Experimental and Computed Absorption and Emission Singlet Excitation Energies (eV), Oscillator Strengths, *f*, and Dipole Moments, μ (D), for 4DEAB−CN and 4DIAB−CN[a]

		4DEAB−CN				4DIAB−CN			
		exp	DFT/MRCI[b]	B3LYP[c]	MPW91[d]	exp	DFT/MRCI[b]	B3LYP[c]	MPW91[d]
					Absorption				
S_0	μ	6.7[e]	7.86	8.13	8.12		7.55	7.28	7.28
			H → L+1[f]	H → L+1	H → L+1		H → L+1	H → L	H → L
				$\pi_{d.} \rightarrow \pi^*_{ph.}$	$\pi_{d.} \rightarrow \pi^*_{ph.}$			$\pi_{d.} \rightarrow \pi^*_{acc.}$	$\pi_{d.} \rightarrow \pi^*_{acc.}$
S_1	ΔE		4.27	4.31	4.41	4.40[g] 4.22[h]	4.31	4.10	4.21
	f		0.030	0.022	0.023		0.014	0.228	0.310
	μ		9.24	11.88	11.73		9.41	14.98	15.08
			H → L[f]	H → L	H → L		H → L	H → L+1	H → L+1
				$\pi_{d.} \rightarrow \pi^*_{acc.}$	$\pi_{d.} \rightarrow \pi^*_{acc.}$			$\pi_{d.} \rightarrow \pi^*_{ph.}$	$\pi_{d.} \rightarrow \pi^*_{ph.}$
S_2	ΔE	4.35[i]	4.56	4.45	4.56		4.39	4.17	4.29
	f		0.707	0.474	0.514		0.609	0.192	0.123
	μ		13.32	10.46	11.47		13.85	14.21	13.52
					Emission				
S_0	μ		5.18	5.58	5.60		5.36	5.63	5.65
	ΔE[j]		0.65	0.49	0.51		0.80	0.27	0.28
			H → L[f]	H → L	H → L		H → L	H → L	H → L
				$n_N \rightarrow \pi^*_{acc.}$	$n_N \rightarrow \pi^*_{acc.}$			$n_N \rightarrow \pi^*_{acc.}$	$n_N \rightarrow \pi^*_{acc.}$
S_1	ΔE	3.27[k]	3.88	3.18	3.34	3.33[g] 3.14[h]	3.80	3.24	3.40
	f		0.001	0.000	0.000		0.000	0.001	0.001
	μ		17.36	20.69	20.29		16.68	20.95	20.55
			H-2 → L[f]	H → L+1	H → L+1		H-2 → L	H → L+1	H → L+1
				$n_N \rightarrow \pi^*_{ph.}$	$n_N \rightarrow \pi^*_{ph.}$			$n_N \rightarrow \pi^*_{ph.}$	$n_N \rightarrow \pi^*_{ph.}$
S_2	ΔE		4.59	4.02	4.22		4.60	4.03	4.24
	f		0.005	0.005	0.001		0.009	0.001	0.001
	μ		7.39	18.70	18.63		5.48	18.90	18.83

[a] Absorption energies have been calculated at the optimized ground-state geometry and emission energies at the perpendicular optimized ground-state geometry (TICT Model). [b] Values from the work of Parusel et al.[51] [c] This work using TDDFT. Excitation energies have been computed with the B3LYP functional using a Bg basis and the geometry has been optimized at the B3LYP level with an Sm basis set. [d] This work using TDDFT. Excitation energies have been computed with the MPW91W91 functional using a Bg basis and the geometry has been optimized at the B3LYP level with an Sm basis set. [e] Value measured in dioxane, see ref. 70. [f] We used here the same notation as the one reported in the work of Parusel et al.[51] [g] Value measured in vapor-phase, see ref. 73. [h] Value measured in *n*-hexane, see ref. 72. [i] Experimental value measured in *n*-hexane, see ref. 91. Estimated gas phase value 4.55 eV. [j] Energy difference between the ground state computed at the equilibrium geometry and at $\theta = 90°$. [k] Value measured in *n*-hexane, see ref. 71.

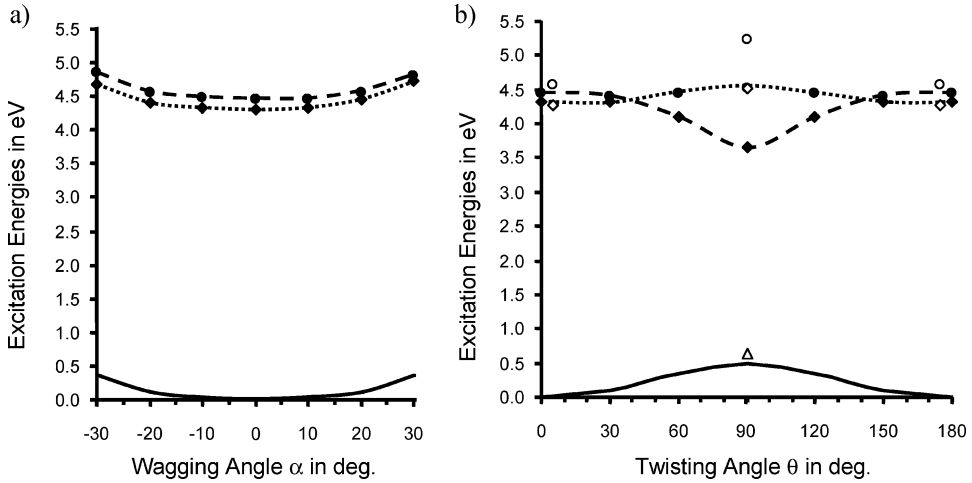

Figure 5. (a) Computed potential energy surface along the wagging angle for 4DEAB−CN. (b) Computed potential energy surface along the twisting angle for 4DEAB−CN. The black symbols represent the adiabatic surfaces, and the various lines (except for the ground state) show the diabatic surfaces. In all curves, the solid line represents the energy profile of the electronic ground state (S_0). The solid diamonds (♦) represent the S_1 excited state, and the solid circles (●) are for the S_2 excited state. The broken line represents transition from the HOMO to the LUMO, and the dotted line is associated with the electronic promotion from the HOMO to LUMO+1. The empty symbols display the DFT/MRCI results.[51]

structure of the computed absorption spectrum for 4DIAB−CN is different from the one of 4DMAB−CN with a first computed excited state having a large oscillator strengh and a charge-transfer nature, which is associated with a $\pi_{donor} \rightarrow \pi^*_{acceptor}$ electronic promotion and a second vertical excited state being related to the $\pi_{donor} \rightarrow \pi^*_{phenyl}$ electronic transition. DFT/MRCI results predict the reverse order of states, the charge transfer being above the locally excited state. Our computed B3LYP and MPW1PW91 excitation energies for the charge-transfer state are below the gas-phase experimental data by 0.30 and 0.19 eV, respectively. This underestimation of the vertical charge-transfer excitation energy has also been observed for the particular case of MMD (see Figure 2).[1] Taking into account the geometrical relaxation should degrade the agreement between theory and experiment. According to our experience in computing vertical charge-transfer excitation energies for pretwisted molecules, hybrid functionals lead to the best agreement with experimental data. On the other hand, DFT/MRCI results predict an absorption energy of 4.39 eV, which is in excellent agreement with gas-phase measurements, 4.40 eV.

C. Emission Spectra for 4DEAB−CN. Parts a and b of Figure 5 present the computed potential energy surface of 4DEAB−CN along the wagging and twisting angle, respectively. In the figures, symbols correspond to the adiabatic potential energy surface and the line (dotted or broken) corresponds to the diabatic potential energy surface. The DFT/MRCI results are also represented in the figures for θ^0 (see Table 2), and for the twisted geometry by empty symbols. In the particular case of 4DEAB−CN, the symmetry of the molecule requires exploration of the wagging angle in both the positive and negative α directions relative to the phenyl plane. Indeed, at the equilibrium ground-state geometry, both ethyl groups adopt a symmetrical bend position on one side of the phenyl plane, and the wagging angle is almost equal to zero.

The potential energy surface of the ground and excited state along the wagging angle present a minimum for α^0 (see Table 2, and Figure 5a). The second excited state of charge-transfer nature does not undergo an energy stabilization and remains above the locally excited state along this motion. Therefore, this mechanism cannot explain the presence of a charge-transfer excited state with a low energy responsible for the abnormal emission.

Along the twisting motion, the potential energy surface of the ground state shows a minimum at $\theta = 0°$ and a maximum for $\theta = 90°$; see Figure 5b. Its dipole moment decreases versus increasing θ (from 0° to 90°) reaching a minimum for the perpendicular conformer. An avoided crossing between the first and second excited states occurs at $\theta = 40°$. The first excited state, which is mainly described by a $\pi_{donor} \rightarrow \pi^*_{phenyl}$ transition at the equilibrium ground-state geometry, will change nature after the crossing point to reach a full charge-transfer decoupling associated with a $n_N \rightarrow \pi^*_{acceptor}$ electronic promotion at $\theta = 90°$. The potential energy surface of the 1S excited state shows a minimum at the perpendicular conformation, whereas the 2S excited-state energy is minimal for the optimized ground-state structure (θ^0). The computed emission energies at the B3LYP−Sm/Bg (3.18 eV) and B3LYP−Sm/MPW1PW91−Bg (3.34 eV) levels compare well with the experimental emission band measured at 3.27 eV in *n*-hexane. The observed dual fluorescence can be explained by the same double mechanism already proposed by Serrano et al.[45] in the particular case of 4DMAB−CN. During the absorption, both the locally and charge-transfer excited states are populated. The charge-transfer excited state will lose energy by a nonradiative process to the locally excited state from which the L_b emission takes place. The locally excited state can also achieve a stabilization by following the hypersurface of the intramolecular twisting motion. From the final perpendicular charge-transfer excited state, an emission occurs that is assigned to the L_a band observed in the fluorescence spectra.

From the perspective of our classification scheme for this family of donor−acceptor systems within the TICT model (Appendix), the 4DEAB−CN molecule belongs to the same group of compounds as 4DMAB−CN (group IV). Experimentally, the majority of the molecules of this group show a dual fluorescence activity in polar and nonpolar solvents, which can be understood by the above mentionned mechanism proposed by Serrano et al.,[45] and which can be rationalized in term of three variables: ΔE^{gap}, ΔE^{1S}, and ΔE^a. Molecules of this group are characterized by a $\Delta E^{gap} < 0$, meaning that the vertical charge-transfer excited state is above the locally excited state, and a $\Delta E^{1S} \leq 0$, which reflects the energy stabilization of the charge-transfer excited state along the twisting angle. ΔE^a is calculated at 0.06 eV at the B3LYP level. It has been computed by taking the energy difference between the first vertical excited

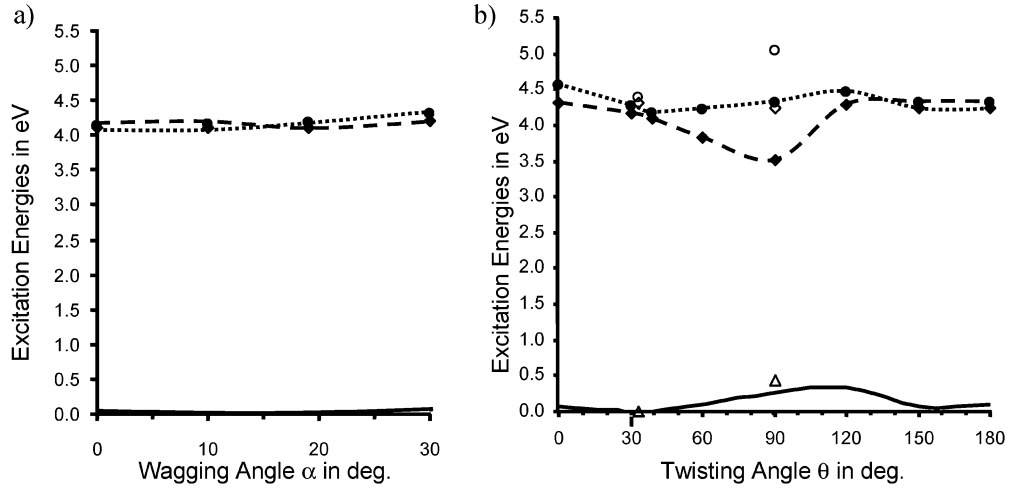

Figure 6. (a) Computed potential energy surface along the wagging angle for 4DIAB−CN. (b) Computed potential energy surface along the twisting angle for 4DIAB−CN. The black symbols represent the adiabatic surfaces, and the various lines (except for the ground state) show the diabatic surfaces. In all curves, the solid line represents the energy profile of the electronic ground-state S_0. The solid diamonds (♦) represent the S_1 excited state, and the solid circles (●) are for the S_2 excited state. The broken line represents transition from the HOMO to the LUMO, and the dotted line is associated with the electronic promotion from the HOMO to LUMO+1. The empty symbols display the DFT/MRCI results.[51]

state and the transition state at $\theta_{crossing} = 40°$ (see Figure 5b) and represents an estimation of the true energy barrier, which would require the knowledge of the energy of the fully optimized twisted charge-transfer excited state, as well as the energy of the optimized transition state along the path from the vertical initial excited state to the final optimized twisted charge-transfer excited state. The height of ΔE^a plays a role in determining the occurrence (or lack thereof) of the dual fluorescence for this particular group and explains why 4MAB−CN is not dual fluorescent even in polar solvent,[4] whereas 4DMAB−CHO is in nonpolar solvents. The increased intensity of the L_a band observed for 4DEAB−CN compared to 4DMAB−CN in the fluorescence spectra cannot be explained by the height of the energy barrier as estimated in the present work, because ΔE^a is equal to 0.06 eV for both molecules at the B3LYP level. More sophisticated calculations that incorporate the explicitly optimized excited-state geometry for each θ angle are necessary to obtain more reliable ΔE^a values.

DFT/MRCI results reported in Figure 5b do not predict a stabilization of the twisting charge-transfer excited state compared to the vertical first excited state. This disagreement between TDDFT and DFT/MRCI results in predicting the stabilization (or not) of the twisted charge-transfer excited state has already been observed for dicyano compounds.[6,52]

TDDFT results predict the occurrence of the dual fluorescence activity for this molecule is agreement with the experimental observations.

D. Emission Spectra for 4DIAB−CN. Parts a and b of Figure 6 present the computed potential energy surface of 4DIAB−CN along the wagging and twisting angles, respectively. The same figure caption as for 4DEAB−CN is used. For 4DIAB−CN, the wagging motion is investigated only according to the half-plane containing $\alpha^0 = 19.33°$ and is varied from 0° to 30°.

For the wagging motion (Figure 6a), the potential energy surface of the first excited state, which has a charge-transfer nature at α^0, presents an avoided crossing with the second excited state ($\pi_{donor} \rightarrow \pi^*_{phenyl}$ transition at α^0) at $\alpha_{crossing} = 15°$. The energy of both 1S and 2S excited states remains almost constant along the wagging angle and no energy stabilization of the charge-transfer excited state is observed along this motion, as in the case of 4DEAB−CN and other related compounds.[3]

For the twisting motion, the structure of the potential energy surface of 4DIAB−CN is expected to be more complex and less symmetric than the one of 4DEAB−CN, because the former has a wagging angle of 19.33°, whereas the latter shows a 3.88° wagging angle. The potential energy surface of the ground electronic state presents the lowest minimum at $\theta^0 = 38°$ and a maximum is computed at 120°. Contrary to 4DEAB−CN, no avoided crossing between the first and second excited state is present in the region where the photochemical process occurs [θ^0, 90] (for $\theta = 140°$ an avoided crossing is present). The potential energy surface of the first excited state, which corresponds to the charge-transfer transition, shows a minimum at the twisted conformation. The energy of the second excited-state characterized by a $\pi_{donor} \rightarrow \pi^*_{acceptor}$ transition shows an energy minimum at the ground-state equilibrium geometry. The energy gap that separates the vertical first and second excited states is computed at 0.07 and 0.09 eV, using the B3LYP−(Sm/Bg) and B3LYP−Sm/MPW1PW91−Bg methods, respectively. The B3LYP−(Sm/Bg) and B3LYP−Sm/MPW1PW91−Bg emission energies ($\theta = 90°$) computed at 3.24 eV and at 3.40 eV, respectively, compare well with vapor phase[73] and *n*-hexane[72] experimental bands at 3.33 and 3.14 eV, respectively.

The dual fluorescence activity of 4DIAB−CN is understood in terms of the small energy gap between the vertical first and second excited state and by a large energy stabilization of the charge-transfer state along the twisting motion without energy barrier. In absorption, both excited states are populated and the L_a emission arises from the relaxed twisted charge-transfer excited state, which is reached along the twisting motion without energy constraint, explaining the presence of a more intense L_a band compared to 4DMAB−CN in nonpolar solvents. In *n*-hexane the quantum yield ratio of 4DIAB−CN is ϕ(CT)/ϕ-(LE) > 27,[72] whereas for 4DMAB−CN, ϕ(CT)/ϕ(LE) = 0.01, in cyclohexane.[71]

4DIAB−CN belongs to group II characterized by a positive ΔE^{gap} and $\Delta\tilde{E}^{1S}$ values (Appendix). 4DIAB−CN has a behavior similar to MMD (see Figure 2) in the gas phase, showing the presence of the abnormal L_a band, which can be understood in both cases by a large $\Delta\tilde{E}^{1S}$ value of 1 eV. However, both molecules behave differently in nonpolar solvents with the presence of the L_b band in the case of 4DIAB−CN, whereas it

SCHEME 1: Schematic Representation of the Various Groups Defined by the Value of ΔE^{gap} ($\Delta E^{gap} = E^{LE} - E^{CT}$ Vertical) and ΔE^{1S} [a]

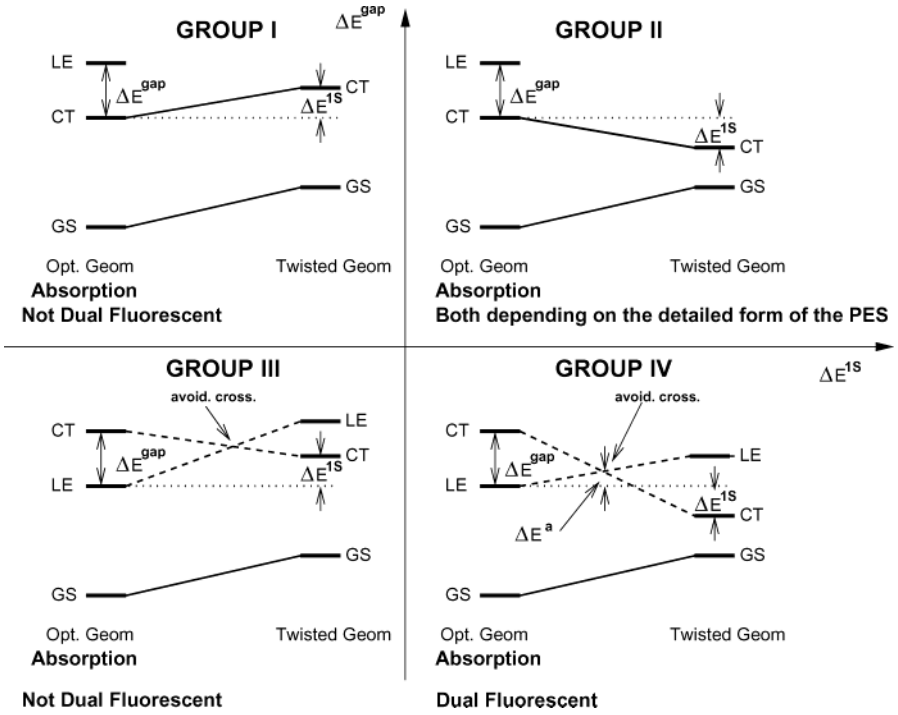

[a] Group I is characterized by $\Delta E^{gap} > 0$ and $\Delta E^{1S} < 0$. Groups II and III are defined by both positive and negative, respectively, values for ΔE^{gap} and ΔE^{1S}. Molecules of group IV have a $\Delta E^{gap} < 0$ and $\Delta E^{1S} > 0$.

is absent for the MMD molecule. This can be explained by a smaller ΔE^{gap} in the former compared to the latter.

DFT/MRCI results predict a slight stabilization by 0.06 eV of the twisted charge-transfer excited state compared to the vertical first excited state, as well as the presence of an avoided crossing between the first and second excited state along the twisting angle. The computed DFT/MRCI emission energy is given at 3.80 eV, whereas measurements lead to a 3.14 eV excitation energy.

IV. Conclusions

In this paper, TDDFT calculations have been performed for the 4DEAB−CN and 4DIAB−CN dual fluorescent molecules. The geometry has been optimized for the electronic ground-state structure using the B3LYP functional combined with the Sm basis set. Excitation energies have been calculated with the B3LYP and MPW1PW91 functionals with the Bg basis set.

The absorption energies computed at the B3LYP and MPW1PW91 levels for 4DEAB−CN compared well to *n*-hexane absorption spectrum with an energy difference of 0.10 and 0.21 eV, respectively. On the other hand, an underestimation of the absorption energy by 0.30 and 0.19 eV, respectively, is obtained in the case of 4DIAB−CN when compared to gas-phase experimental measurements. In the case of 4DIAB−CN, the absorption energies computed with the DFT/MRCI method are in better agreement with the experimental gas-phase data than TDDFT ones, whereas both methods lead to results of comparable quality for 4DEAB−CN. Increasing the alkyl chain size from 4DMAB−CN, to 4DEAB−CN and 4DIAB−CN reduces the energy gap between the vertical locally and charge-transfer excited states from +0.25 to +0.14 and −0.06 eV, respectively.

The dual fluorescence observed for 4DEAB−CN is explained within the twisting intramolecular charge-transfer model by the double mechanism already proposed by Serrano et al.[45] The B3LYP and MPW1PW91 computed emission energies show a difference of −0.09 and +0.07 eV with *n*-hexane measurements.

The dual fluorescence of 4DIAB−CN is also understood within the TICT model by the presence of a small energy gap between the vertical first and second excited state. The L_b band corresponds to an emission from the relaxed second excited state, and the L_a band arises from the twisted charge-transfer excited state. The energy difference between the B3LYP and MPW1PW91 computed emission energies and gas-phase experimental data is given at −0.09 and +0.07 eV, respectively.

For both compounds, the potential energy surface along the wagging angle has been investigated and does not lead to the presence of an energy stabilization of the charge-transfer excited state, which would explain the dual fluorescence activity experimentally observed for both compounds.

The TDDFT method, which has been previously used to describe the emission property of small molecules (having a smaller donor group, typically a dimethylamino group), has proved to be successful in describing the fluorescence activity of larger systems, such as the ones of this study. Furthermore, the classification that has been proposed in ref 2 is also valid for the present compounds with longer alkyl chain size than the previously studied molecules and gives a reliable prediction of the occurrence of the dual fluorescence activity, in agreement with the experimental findings.

This study reinforces the validity of the TICT model as a possible mechanism that explains the dual fluorescence for these donor−acceptor systems.

Acknowledgment. C.J.J. thanks Dr. H. Jödicke for interesting and stimulating discussions and for helping in creating the figures as well as for his continuous financial support. C.J.J. also thanks Dr. N. Desmarais for reading this manuscript.

Appendix

We review the four category classification previously presented in ref 2; see Scheme 1. We have proposed that the behavior of dual fluorescent compounds of the type discussed in this and our previous articles may be predicted on the basis of three parameters: $\Delta E^{gap} = E^{LE} - E^{CT}$, the difference of vertical excitation energies to the local excited and charge-transfer state; $\Delta\tilde{E}^{1S} = (90/|\theta^0 - (\theta = 90)|)\Delta E^{1S}$, the relative energies of the twisted ($\theta = 90°$) charge-transfer state and the first vertical excited state ($\Delta E^{1S} = E^{1S}(\theta = \theta^0) - E^{CT}(\theta = 90°)$) normalized to 90°. The quantity ΔE^a is the height of the energy barrier along the twisting path in the case of group IV. According to this scheme (and consistent with all known facts), systems belonging to the same group show similar computed potential energy surfaces and present the same fluorescence behavior, except in the case of group II where three subcategories have been characterized according to the size of ΔE^{gap} and $\Delta\tilde{E}^{1S}$. Molecules, like MMD, with a large ΔE^{gap} and $\Delta\tilde{E}^{1S}$ show only the abnormal L_a emission in the gas phase. Compounds, like NMC7, with a small ΔE^{gap} and $\Delta\tilde{E}^{1S}$ (close to 0 eV) show a dual fluorescence activity in polar solvents and only the L_b band in nonpolar solvents. Systems with intermediate $\Delta\tilde{E}^{1S}$ and ΔE^{gap} values have been observed to have dual fluorescence in polar solvents (nonpolar data have not been reported for the compound previously investigated; see ref 2).

References and Notes

(1) Jamorski, C.; Foresman, J. B.; Thilgen, C.; Lüthi, H.-P. *J. Chem. Phys.* **2002**, *116*, 8761.

(2) Jamorski, C. J.; Lüthi, H.-P. *J. Chem. Phys.*, in press.

(3) Jamorski, C. J.; Lüthi, H.-P. *J. Am. Chem. Soc.* **2003**, *125*, 252.

(4) Jamorski, C. J.; Lüthi, H.-P. *J. Chem. Phys.* **2002**, *117*, 4146.

(5) Jamorski, C. J.; Lüthi, H.-P. *J. Chem. Phys.* **2003**, *117*, 4157.

(6) Jamorski, C. J.; Lüthi, H.-P. *Chem. Phys. Lett.* **2003**, *368*, 561.

(7) (a) Lippert, E.; Lüppert, W.; Moll, F.; Nägele, W.; Boos, H.; Prigge, H.; Seibold-Blankenstein, I. *Angew. Chem.* **1961**, *6*, *7*, 3.95. (b) Lippert, E.; Lüder, W.; Boss, H. *Adv. Mol. Spectrosc.* **1962**, 443.

(8) Bosshard, C.; Sutter, K.; Prêtre, P.; Hulliger, J.; Flörsheimer, M.; Kaatz, P.; Günter, P. *Organic Nonlinear Optical Materials*; Advances in Nonlinear Optics, Vol. 1; Gordon and Breach Publichers: New York, 1995.

(9) Kippelen, B.; Lackritz, H. S.; Claus, R. O. *Organic Nonlinear Optical Material and devices*; Materials Research Society: Warrendale, PA, 1999.

(10) Lakowicz, J. P. *Principles of Fluorescence Spectroscopy*, 2nd ed.; Kluwer Academic: Hongham, 1999.

(11) (a) La Chair, J. J. *Angew. Chem., Int. Ed. Engl.* **1999**, *38*, 3047. (b) *Angew. Chem., Int. Ed. Engl.* **1998**, *37*, 325. (c) *Angew. Chem., Int. Ed. Engl.* **1998**, *110*, 339. (d) *J. Am. Chem. Soc.* **1997**, *119*, 7676.

(12) Khalil, O.; Hofedt, R. H.; McGlynn, S. P. *Chem. Phys. Lett.* **1972**, *17*, 479.

(13) Dodiuk, H.; Kosower, E. M. *Chem. Phys. Lett.* **1975**, *44*, 253. Dodiuk, H. *J. Am. Chem. Soc.* **1976**, *98*, 924.

(14) Sobolewski, A. L.; Domcke, W. *Chem. Phys. Lett.* **1996**, *259*, 119.

(15) Sobolewski, A. L.; Domcke, W. *Chem. Phys. Lett.* **1996**, *250*, 428.

(16) Sobolewski, A. L.; Sudholt, W.; Domcke, W. *J. Phys. Chem. A* **1998**, *102*, 2716.

(17) Chandross, E. A. In *Exciplex*; Gordon, M., Ware, W. R., Eds.; Academic Press: New York, 1975; p 187.

(18) Visser, R. J.; Varma, C. A. *J. Chem. Soc., Faraday Trans. 2* **1980**, *76*, 453. Visser, R. J.; Weisenborn, P. C. M.; Varma, C. A. *Chem. Phys. Lett.* **1985**, *113*, 330. Weisenborn, P. C. M.; Varma, C. A.; de Haas, M. P.; Warman, J. M. *Chem. Phys. Lett.* **1986**, *129*, 560.

(19) (a) Rotkiewicz, K.; Grellmann, K. H.; Grabowski, Z. R. *Chem. Phys. Lett.* **1973**, *19*, 315. (b) *Chem. Phys. Lett.* **1973**, *21*, 212.

(20) Grabowski, Z. R.; Rotkiewicz, K.; Siemiarczuk, A.; Cowley, D. J.; Baumann, W. *N. J. Chim.* **1979**, *3*, 443.

(21) Zachariasse, K.; van der Haar, T.; Hebecker, A.; Leinhos, U.; Kühnle, W. *Pure Appl. Chem.* **1993**, *65*, 1745.

(22) Zachariasse, K. A.; Grobys, M.; von der Haar, T.; Hebecker, A.; Il'ichev, Y. V.; Jiang, Y.-B.; Morawski, O.; Kühnle, W. *J. Photochem. Photobiol. A: Chem.* **1996**, *102*, 59.

(23) Zachariasse, K. A.; Grobys, M.; Tauer, E. *Chem. Phys. Lett.* **1997**, *274*, 372.

(24) Il'ichev, Y. V.; Kühnle, W.; Zachariasse, K. A. *J. Phys. Chem. A* **1998**, *102*, 5670.

(25) Zachariasse, K. A.; Grobys, M.; von der Haar, T.; Hebecker, A.; Il'ichev, Y. V.; Morawski, O.; Rücker, I.; Kühnle, W. *J. Photochem. Photobiol. A: Chem.* **1997**, *105*, 373.

(26) von der Haar, T.; Hebecker, A.; Il'ichev, Y. V.; Jiang, Y.-B.; Kühnle, W.; Zachariasse, K. A. *Recl. Trav. Chim. Pays Bas* **1995**, *114*, 430.

(27) Kwok, W. M.; Ma, C.; Matousek, P.; Parker, A. W.; Phillips, D.; Toner, W. T.; Towrie, M. *Chem. Phys. Lett.* **2000**, *322*, 395.

(28) Dreyer, J.; Kummrow, A. *J. Am. Chem. Soc.* **2000**, *122*, 2577.

(29) Okamoto, H.; Inishi, H.; Nakamura, Y.; Kohtani, S.; Nakagaki, R. *Chem. Phys.* **2000**, *260*, 193.

(30) Okamoto, H. *J. Phys. Chem. A* **2000**, *104*, 4182.

(31) Okamoto, H.; Inishi, H.; Nakamura, Y.; Kohtani, S.; Nakagaki, R. *J. Phys. Chem. A* **2001**, *105*, 4182.

(32) Kato, S.; Amatasu, Y. *J. Chem. Phys.* **1990**, *92*, 7241.

(33) Broo, A.; Zerner, M. C. *Chem. Phys. Lett.* **1994**, *227*, 551.

(34) Gorse, A.-D.; Pesquer, M. *J. Phys. Chem.* **1995**, *99*, 4039.

(35) Scholes, G. D.; Phillips, D.; Gould, I. R. *Chem. Phys. Lett.* **1997**, *266*, 521.

(36) Gedeck, P.; Schneider, S. J. *J. Photochem. Photobiol. A: Chem.* **1997**, *105*, 165.

(37) Scholes, G. D.; Gould, I. R.; Parker, A. W.; Philips, D. *Chem. Phys.* **1998**, *234*, 21.

(38) Purkayastha, P.; Bhattacharyya, P. K.; Bera, S. C.; Chattapadhyay, N. *Phys. Chem. Chem. Phys.* **1999**, *1*, 3253.

(39) Gedeck, P.; Schneider, S. J. *J. Photochem. Photobiol. A: Chem* **1999**, *121*, 7.

(40) Mennucci, B.; Toniolo, A.; Tomasi, J. *J. Am. Chem. Soc.* **2000**, *112*, 10621.

(41) Cammi, R.; Mennucci, B.; Tomasi, J. *J. Phys. Chem. A* **2000**, *104*, 5631.

(42) Sudholt, W. Staib, A.; Sobolewski, A. L.; Domcke, W. *Phys. Chem. Chem. Phys.* **2000**, *2*, 4341.

(43) Bulliard, C.; Allan, M.; Wirtz, G.; Haselbach, E.; Zachariasse, K. A.; Detzer, N.; Grimme, S. *J. Phys. Chem. A* **1999**, *103*, 7766.

(44) Gorse, A.-D.; Pesquer, M. *J. Mol. Struct.* **1993**, *281*, 21.

(45) Serrano-Andrés, L.; Merchán, M.; Roos, B. J.; Lindh, R. *J. Am. Chem. Soc.* **1995**, *117*, 3189.

(46) Sudholt, W.; Sobolewski, A.; Domcke, W. *Chem. Phys.* **1999**, *240*, 9.

(47) Parusel, A. B. J.; Köhler, G.; Nooijen, M. *J. Phys. Chem. A* **1999**, *103*, 4056.

(48) Parusel, A. B. J.; Köhler, G.; Grimme, S. *J. Phys. Chem. A* **1998**, *102*, 6297.

(49) Parusel, A. B. J. *Phys. Chem. Chem. Phys.* **2000**, *24*, 5545.

(50) Parusel, A. B. J. *Chem. Phys. Lett.* **2001**, *340*, 531.

(51) Parusel, A. B. J.; Köhler, G. *Int. J. Quantum Chem.* **2001**, *84*, 149.

(52) Parusel, A. B. J.; Schamschule, R.; Köhler, G. *Z. Phys. Chem.* **2002**, *216*, 361.

(53) Parusel, A. B. J.; Rettig, W.; Sudholt, W. *J. Phys. Chem. A* **2002**, *106*, 804.

(54) Andersson, K.; Malmqvist, P.-Å.; Roos, B. O.; Sadlej, A. J.; Wolinski, K. J. *J. Phys. Chem.* **1990**, *94*, 5483.

(55) Andersson, K.; Malmqvist, P.-Å.; Roos, B. O. *J. Chem. Phys.* **1992**, *92*, 1218.

(56) Nooijen, M.; Bartlett, R. J. *J. Chem. Phys.* **1997**, *106*, 6441.

(57) Nooijen, M.; Bartlett, R. J. *J. Chem. Phys.* **1997**, *107*, 6812.

(58) Grimme, S. *Chem. Phys. Lett.* **1996**, *259*, 128.

(59) Grimme, S.; Waletzke, M. J. *J. Chem. Phys.* **1999**, *111*, 5645.

(60) Furcher, F. Poster PA84 presented in WATOC 2002.

(61) Foresman, J. B.; Head-Gordon, M.; Pople, J. A.; Firsch, M. J. *J. Phys. Chem.* **1992**, *96*, 135.

(62) Zilberg, S.; Haas, Y. *J. Phys. Chem. A* **2002**, *106*, 1.

(63) Proppe, B.; Merchán, M.; Serrano-Andrés, L. *J. Phys. Chem. A* **2000**, *104*, 1608.

(64) Gross, E. K. U.; Kohn, W. *Adv. Quantum Chem.* **1990**, *21*, 255.

(65) Gross, E. K. U.; Ullrich, C. A.; Gossmann, U. J. In *Density Functional Theory*; Gross, E. K. U., Dreizler, R. M., Eds.; NATA ASI Series; Plenum: New York, 1994; p 149.

(66) Casida, M. E.; Jamorski, C.; Bohr, F.; Guan, J.; Salahub, D. R. In *Theoretical and Computational Modeling of NLO and Electronic Materials*; Karna, A. P., Yeates, A. T., Eds.; Proceedings of ACS Symposium, Washington, DC, 1994; American Chemical Society: Washington, DC, 1996; p 145.

(67) Casida, M. E. In *Recent Advances in Density Functional Methods, Part I*; Chong, D. P., Ed.; World Scientific: Singapore, 1995; p 155.

(68) Jamorski, C.; Casida, M. E.; Salahub, D. R. *J. Chem. Phys.* **1996**, *104*, 5134.

(69) Bauernschmitt, R.; Ahlrichs, R. *Chem. Phys. Lett.* **1996**, *256*, 454.

(70) Bauman, W.; Bischof, H.; Frohling, J. C.; Brittinger, C.; Rettig, W.; Rotkiewicz, K. J. *J. Photochem. Photobiol. A: Chem* **1992**, *64*, 49.

(71) Schuddeboom, W.; Jonker, S. A.; Warman, J. M.; Leinhos, U.; Kühnle, W.; Zachariasse, K. A. *J. Phys. Chem.* **1992**, *96*, 10809.
(72) Demeter, A.; Druzhinin, S.; George, M.; Haselbach, E.; Roulin, J.-L.; Zachariasse, K. A. *Chem. Phys. Lett.* **2000**, *323*, 351.
(73) Daum, R.; Druzhinin, S.; Ernst, D.; Rupp, L.; Scroeger, J.; Zachariasse, K. A. *J. Chem. Phys.* **2001**, *341*, 272.
(74) Rettig, W. *Angew. Chem., Int. Ed. Engl.* **1986**, *25*, 971.
(75) Druzhinin, S. I.; Demeter, A.; Zachariasse, K. A. *Chem. Phys. Lett.* **2001**, *347*, 421.
(76) Frisch, M. J.; Trucks, G. W.; Schlegel, H. B.; Scuseria, G. E.; Robb, M. A.; Cheeseman, J. R.; Zakrzewski, V. G.; Montgomery, J. A., Jr.; Stratmann, R. E.; Burant, J. C.; Dapprich, S.; Millam, J. M.; Daniels, A. D.; Kudin, K. N.; Strain, M. C.; Farkas, O.; Tomasi, J.; Barone, V.; Cossi, M.; Cammi, R.; Mennucci, B.; Pomelli, C.; Adamo, C.; Clifford, S.; Ochterski, J.; Petersson, G. A.; Ayala, P. Y.; Cui, Q.; Morokuma, K.; Malick, D. K.; Rabuck, A. D.; Raghavachari, K.; Foresman, J. B.; Cioslowski, J.; Ortiz, J. V.; Baboul, A. G.; Stefanov, B. B.; Liu, G.; Liashenko, A.; Piskorz, P.; Komaromi, I.; Gomperts, R.; Martin, R. L.; Fox, D. J.; Keith, T.; Al-Laham, M. A.; Peng, C. Y.; Nanayakkara, A.; Challacombe, M.; Gill, P. M. W.; Johnson, B.; Chen, W.; Wong, M. W.; Andres, J. L.; Gonzalez, C.; Head-Gordon, M.; Replogle, E. S.; Pople, J. A. *Gaussian98*, revision X.X; Gaussian, Inc.: Pittsburgh, PA, 1998.
(77) Hehre, W. J.; Ditchfield, R.; Pople, J. A. *J. Chem. Phys.* **1972**, *56*, 2257.
(78) Krishnan, R.; Binkley, J. S.; Seeger, R.; Pople, J. A. *J. Chem. Phys.* **1980**, *72*, 650.
(79) Frisch, M. J.; Pople, J. A.; Binkley, J. S. *J. Chem. Phys.* **1984**, *80*, 3265.
(80) Becke, A. D. *J. Chem. Phys.* **1993**, *98*, 5648.
(81) Adamo, C.; Barone, V. *J. Chem. Phys.* **1998**, *108*, 664.
(82) Stratmann, R. E.; Scuseria, G. E.; Frisch, M. J. *J. Chem. Phys.* **1998**, *109*, 8218.
(83) Casida, M. E.; Jamorski, C.; Casida, K. C.; Salahub, D. R. *J. Chem. Phys.* **1998**, *11*, 4439.
(84) Van Caillie, C.; Amos, R. D. *Chem. Phys. Lett.* **1999**, *308*, 249.
(85) Van Caillie, C.; Amos, R. D. *Chem. Phys. Lett.* **2000**, *317*, 159.
(86) Furcher, F.; Ahlrichs, R. *J. Chem. Phys.* **2002**, *117*, 7433.
(87) Heine, A.; Herbst-Irmer, R.; Stalke, D.; Kühnle, W.; Zachariasse, K. A. *Acta Crystallogr.* **1994**, *B50*, 363.
(88) Kajimoto, O.; Yokohama, H.; Ooshima, Y.; Endo, Y. *Chem. Phys. Lett.* **1991**, *179*, 455.
(89) von Büllow, R.; Stalke, D.; Zachariasse, K. A. Unpublished.
(90) Rettig, W.; Gleiter, R. J. *J. Phys. Chem.* **1985**, *89*, 4676.
(91) Rettig, W. *J. Luminesc.* **1980**, *26*, 21.